Highly sensitive and selective CO sensor using a 2.33 µm diode laser and wavelength modulation spectroscopy

RUYUE CUI,[1,2] LEI DONG,[1,2,*] HONGPENG WU,[1,2] SHANGZHI LI,[1,2] LEI ZHANG,[1,2] WEIGUANG MA,[1,2] WANGBAO YIN,[1,2] LIANTUAN XIAO,[1,2] SUOTANG JIA,[1,2] AND FRANK K. TITTEL[3]

[1]*State Key Laboratory of Quantum Optics and Quantum Optics Devices, Institute of Laser Spectroscopy, Shanxi University, Taiyuan 030006, China*
[2]*Collaborative Innovation Center of Extreme Optics, Shanxi University, Taiyuan 030006, China*
[3]*Department of Electrical and Computer Engineering, Rice University, 6100 Main Street, Houston, TX 77005, USA*
*donglei@sxu.edu.cn

Abstract: A ppm-level CO sensor based on a $2f$ wavelength modulation spectroscopy ($2f$-WMS) technique was developed for the application of SF_6 decomposition analysis in an electric power system. A detailed investigation of the optimum target line selection was carried out to avoid spectral interference from high purity SF_6 in a wide wavelength range. A diode laser emitting at 2.33 µm and a 14.5-m multipass gas cell (MGC) was employed to target the $R(6)$ line of the CO first overtone band and increase the optical path, respectively, thus resulting in a minimum detection sensitivity of 1 ppm. A Levenberg-Marquardt nonlinear least-squares fit algorithm makes full use of the information from all data points of the $2f$ spectrum and as a result, a measurement precision of ~40 ppb was achieved with a data update rate of 0.6 s. The sensor performance was also evaluated in terms of the gas flow rate, stability, and linearity. The results showed that the best operating condition with a precision of 6 ppb can be achieved by increasing the gas flow rate to the value that matches the optimum averaging time of 48 s.

1. Introduction

Sulfur hexafluoride (SF_6) has been widely used as an insulating medium in electric power transmission equipment of a >110 kV high-voltage power grid, such as gas-insulated switchgear (GIS) and gas circuit breakers (GCBs). The monitoring of the operating condition of electric power transmission equipment is vital to ensure failure-free operation of the electric power transmission lines. The online detection for SF_6 decomposition is an effective means for fault early warning of electric power transmission equipment, which is based on the fact that SF_6 can be decomposed in the case of superheating and a partial discharge (PD) caused by latent inner insulation defects. In this process, various sulfur-containing, fluorine-containing compounds, such as SF_4, HF, SO_2F_2, SOF_2, SO_2, CO_2,CO, SF_4, are generated via a reaction between water, oxygen, metal vapor or other impurities [1–5]. These decomposition gases can be employed as indicator gases to locate and identify fault types and their locations.

Carbon monoxide (CO) is one of the indicator gases indicating equipment overheating. When the CO content increases in the environment of a low concentration level of sulfur-containing compounds, it implies that a low-temperature overheating occurred inside the equipment, due to the fact that the organic insulating materials with low thermal decomposition temperature, such as polyester ethylene, insulating paper and insulating paint, slowly release CO gas at low-temperature overheating. Therefore, the CO content can identify the low-temperature overheating fault of the equipment. Moreover, the concentration

level of CO increases with cumulative equipment operation time increasing. The operation time of the equipment can be estimated. For example, for 1,100 kV GIS equipment, the concentration levels are <20 ppm under normal operating conditions [6]. Therefore, there is considerable interest in developing an online, cost-effective and ppm-level CO sensor for SF_6 decomposition analysis.

Trace gas detection based on tunable diode laser absorption spectroscopy (TDLAS) is a versatile technique for analysis of gas compositions, since it offers narrow spectral resolution, high sensitivity and fast response time, which permits online monitoring of target gas concentrations [7–12]. The performance of TDLAS based sensors is dependent on the availability of suitable laser sources, such as single mode laser diodes in the near-infrared (near-IR) wavelength up to ~3 μm, quantum cascade lasers (QCLs) in the mid-infrared (mid-IR) region beyond ~3.7 μm and GaSb-based interband cascade lasers (ICLs) emitting in the 3-4 μm wavelength. F. Wang et al. [13] used the TDLAS technique and a 1.58-μm VCSEL diode laser as a radiation source to monitor CO concentration levels. A detection sensitivity of ~200 ppm was achieved. In 2009, X. Chao et al. [14], developed a TDLAS based sensor for CO detection by use of a distributed feedback (DFB) diode laser operating at 2.3 μm, which resulted in a detection sensitivity of 3 ppm. In 2017, J. Dang et al. [15] employed a high-power, continuous wave (CW), distributed feedback (DFB) QCL emitting at 4.7 μm and a 1.6-m multipass gas cell (MGC) to detect CO, which resulted in a minimum detection limit of 26 ppb. Furthermore, R. Ghorbani et al. [16] reported a compact sensor for CO detection by employing a 4-m circular MGC with an ICL emitting at 4.69 μm. The detection limit obtained was 9 ppb. Although a ppb-level CO sensor was achieved by use of the TDLAS technique with a mid-IR QCL or ICL targeting the strongest fundamental absorption band, these gas sensors were designed to operate in a nitrogen (N_2) buffer gas environment. Hence they are unsuitable for use in electric power transmission equipment since high SF_6 concentration levels have abundant absorption spectra in the IR region.

In this paper, we describe a TDLAS based CO sensor based on a CW, DFB diode laser with low power consumption emitting at 2.33 μm for SF_6 decomposition detection. A careful investigation of the line selection was carried out and a compromise is made in terms of cross-response, cost-effectiveness and detection sensitivity. 2f wavelength modulation spectroscopy (2f-WMS) and a 14.5-m Herriot MGC were employed to achieve a high detection sensitivity. The optical sensor system using the selected target spectrum results in a ppm-level CO minimum detection limit in a SF_6 buffer gas environment, which can be applied to the online monitoring of a low-temperature overheating fault inside electric power transmission equipment.

2. Line selection

The selection of gas absorption line is crucial for the detection of gas concentration levels using narrow linewidth lasers, which affects both the resolution and sensitivity of a detection system. In general, the selection of gas absorption line is mainly determined by two main aspects. First the wavelength where the selected absorption line is located must be covered by commercially available laser sources. Secondly, the selected absorption line must have sufficient line strength to achieve the required sensitivity and simultaneously avoid interference with other existing gases. The absorption band of CO, which has been employed to determine the CO concentration levels, includes the fundamental vibration band near 4.6 μm [17,18], the first overtone band near 2.3 μm [19,20] and the second overtone band near 1.55 μm [21]. The fundamental vibration band near 4.6 μm possesses the strongest absorption coefficient and their wavelength can be reached by lead-salt lasers [22] and quantum cascade lasers (QCLs) [23] with a ppb-level detection sensitivity. Both the first and second overtone bands near 2.3 μm and 1.55 μm can be covered by cost-efficient DFB diode lasers, whose detection sensitivities, however, only reach ppm CO concentration levels, due

to the fact that their absorption coefficients are weaker by two and four orders of magnitude than the fundamental vibration band, respectively.

To select an interference-free CO absorption line, the absorption spectrum of SF_6 has to be investigated, since a TDLAS based CO sensor for SF_6 decomposition detection is required to operate in the environment of a SF_6 buffer gas. The HITRAN database provides the line parameters regarding the strong v_3 band of SF_6 at 10.5 μm. However, the concentration of SF_6 in an electric power system is usually >99.8%. As a result, some weaker unidentified absorption bands of SF_6 between 2.5 μm and 10 μm cannot be disregarded in the case of high SF_6 concentration levels. A Fourier transform infrared (FTIR) spectrometer (Thermofisher Nicolet IS50) equipped with a special multipass gas cell of 10 m path length was employed to investigate the interference between the absorption lines of CO and SF_6. Pure SF_6 (99.99%) was introduced into the gas cell first at atmospheric pressure. The dashed navy line in Fig. 1 depicts the absorption spectra of pure SF_6 between 2 and 5.5 μm. The pure SF_6 spectra show an absorption band at a wavelength of >2.5 μm. Next a 1,000 ppm $CO:N_2$ mixture gas was filled into the gas cell after flushing the gas cell with a pure N_2 flow. The red line in Fig. 1 represents the fundamental vibration and first overtone bands of 1,000 ppm CO located at 4.6 μm and 2.33 μm, respectively. The absorption band near 4.9 μm is due to pentacarbonyl-iron ($Fe(CO)_5$) which is produced by the reaction between CO and the gas cylinder material iron. The fundamental vibration band of CO near 4.6 μm was strongly interfered with SF_6 spectra. Since the CO spectra are from 1000 ppm $CO:N_2$ mixture gas, it is a challenge to identify the variation of a ppm concentration level in the presence of a large background interference from SF_6. Therefore the fundamental vibration band is not suitable for the CO detection in electric power systems. The first overtone band of CO between 2.3 and 2.4 μm is 100 times weaker than the fundamental vibration band. No SF_6 spectra are observed as shown in the inset of Fig. 1. The first overtone band of CO is interference free from SF_6 spectra. We selected $R(6)$ transitions located at 4285.01 cm^{-1} in the first overtone band of CO as the target detection line, since it has the stronger absorption linestrength of 8.32×10^{-2} cm^{-2}/atm. Thus a ppm-level detection sensitivity can be expected based on the experience of the CO sensor operating with a N_2 buffer gas in this wavelength region, which can meet the requirements for a SF_6 decomposition analysis.

A CW DFB antimonide diode laser was employed as the light source from nanoplus Nanosystems and Technologies GmbH (http://www.nanoplus.com/) emitting single-mode radiation at a center wavelength of 2333.7 nm, in order to target the selected $R(6)$ absorption line. The output wavelength and power of the diode laser were characterized, respectively, at different laser currents using the FTIR spectrometer and a power meter (Ophir Optironica, model 3A). The wavelength of the diode laser can be tuned between 4282 cm^{-1} and 4290 cm^{-1}, as shown in Fig. 2(a). The wavelength tuning range covers the selected $R(6)$ line plotted as a black line in Fig. 2(a). The current and temperature tuning coefficients of the diode laser are −0.049 cm^{-1}/mA and −0.403cm^{-1}/°C, respectively. An operating current and temperature of 85 mA and 31.3 °C were selected. An operating temperature higher than room temperature is helpful to decrease the power consumption of the laser temperature control, since a heating process has a higher efficiency than a cooling process. The measured L-I-V (light-current-voltage) curve at an operating temperature of 31.3 °C is shown in Fig. 2(b). The output optical power is 2.2 mW with a forward voltage of 1.1 V when the diode laser was operated at a current of 85 mA. In this condition, the power consumption of the diode laser is only 90 mW.
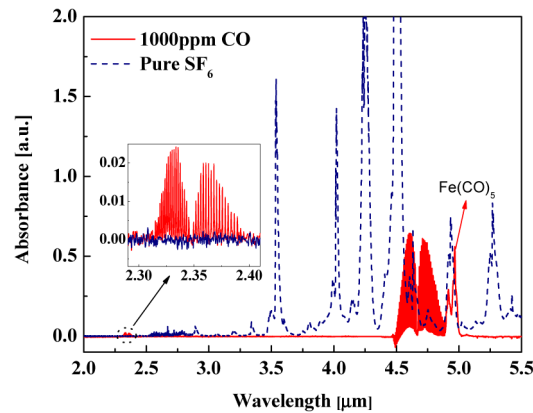
Fig. 1. Pure SF_6 absorption spectra (dashed navy line) and 1,000 ppm CO absorption spectra (red line) in N_2 buffer gas obtained by a FTIR spectrometer with a 10-m multipass gas cell (spectral resolution 0.5 cm^{-1}). Inset: enlarged view of the first overtone band of 1,000 ppm CO and a SF_6 background.
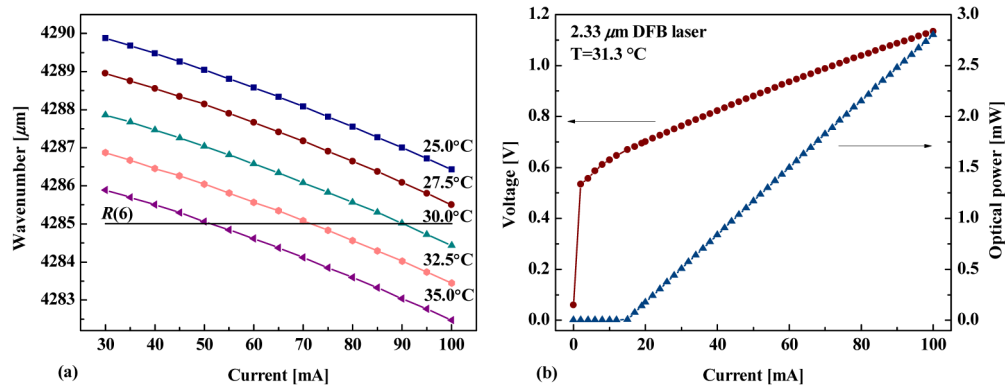

Fig. 2. (a) Diode laser wavelength as a function of current tuning at five different operating temperatures. (b) L-I-V curve of the 2.33 μm CW, DFB diode laser.

3. Sensor design

The schematic of the CO sensor system is depicted in Fig. 3. The CO sensor system consisted of three parts: an optical unit, a control unit and a gas handling unit. In the optical unit, the CW-DFB diode laser operating at 2.3 μm was collimated to a parallel beam with a diameter of 7.3 mm by a collimator (Thorlabs, F810APC-2000). A semiconductor laser diode (alignment laser) emitting 635 nm visible light is used as the guide beam for the invisible infrared (IR) light beam. The light paths of the visible and IR laser beams, were overlapped by means of a flip mirror. Two plane mirrors, Mirror 1 (M1) and Mirror 2 (M2), converted the laser beams from the forward to backward propagation to fold the necessary light path and minimize the size of the optical part. A Herriot MGC was used to enhance the detection sensitivity, which has an invar enclosure with a typical mean coefficient of thermal expansion of 10^{-6}/°C. An effective optical path length of 14.5 m was obtained after 52 beam passes in the Herriot MGC. The exiting, IR beam from the MGC was subsequently received by an InGaAs detector (Thorlabs, PDA 10D-EC). To couple the invisible IR into the MGC, the flip mirror first reflected the visible guide beam into the MGC. A circle pattern with a designed 14.5 m light path can be achieved by adjusting the horizontal and vertical angles of mirrors, M1 and M2. Then the flip mirror was removed in order to introduce the invisible IR beam into the MGC. In this way, the invisible IR beam has the same optical pattern and light

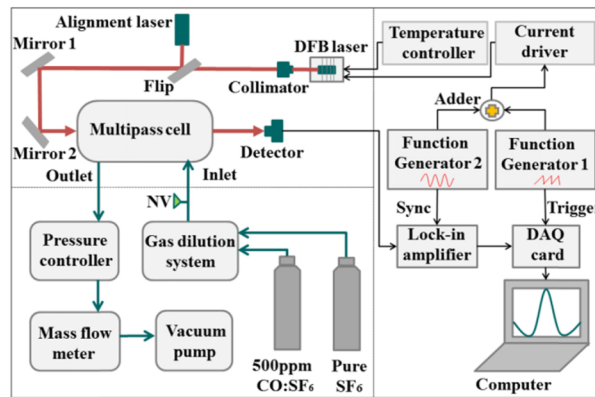path as the visible guide beam due to the fact that the two light paths were overlapped in advance.

Fig. 3. Schematic of CO gas sensor system for SF_6 decomposition analysis.

In the control unit, a current driver (Newport, ILX-3220) and a commercial temperature controller (Thorlabs, model TED 200C) were employed to operate the central wavelength of the DFB laser at the $R(6)$ transitions located at 4285.01 cm^{-1} in the first overtone band of CO. $2f$ based wavelength modulated spectroscopy ($2f$-WMS) was used to obtain a high detection sensitivity. Function generator 1 generated a saw tooth wave to scan the laser wavelength, while function generator 2 generated a sine wave with a small amplitude to dither the laser wavelength. The two waves from function generator 1 and 2 were added by a custom made electrical adder and then sent to the modulation port of the current driver. The output signal from the InGaAs detector (Throlabs, PDA10D-EC) was sent to a lock-in amplifier (Stanford, SR830). The lock-in amplifier demodulated the signal in the $2f$ mode with respect to the sync signal from function generator 2. An acquisition system consisting of a DAQ card and a laptop was triggered by function generator 1 to acquire the $2f$ spectra from the InGaAs detector.

The gas handling unit consisted of standard gas cylinders, a gas dilution system, a pressure controller, a mass flow meter and a vacuum pump. The gas dilution system diluted a certificated 500-ppm CO:SF_6 mixture gas (Air Products) with a 99.99% pure SF_6 gas (Air Products) to produce the CO:SF_6 mixture gases with the different concentration levels. The 99.99% pure SF_6 gas contains an unavoidable impurity of 3-ppm CO, which was verified by the supplier and was taken into account in all gas dilution processes. A needle valve was placed upstream to the MGC to adjust the gas flow, while the pressure controller and vacuum pump were placed downstream to the MGC in order to maintain a constant pressure in the MGC. A mass flow meter was inserted between the pressure controller and vacuum pump to monitor the gas flow.

4. Experimental results and discussions

4.1 Modulation depth and gas pressure optimization

With the $2f$-WMS based CO sensor, the pressure-dependent absorption linewidth must match the modulation depth of the laser, since the maximum peak of the $2f$ signal occurs at the optimal modulation depth and gas pressure [24,25]. A 20-ppm CO:SF_6 mixture gas produced by the gas dilution system was filled into the MGC. The $2f$ signal amplitudes with a modulation depth between 0.014 cm^{-1} and 0.19 cm^{-1} and a pressure range of 200-700 Torr were acquired and depicted in Fig. 4. The $2f$ signal amplitudes vary significantly with modulation depth and gas pressure. The $2f$ signal amplitudes from the different pressures

linearly increase together with the modulation depth increasing in the range of 0.014-0.07 cm^{-1}. When the modulation depth is >0.07 cm^{-1}, the 2f signal amplitudes for the different gas pressures reach the maximum value in turn and then decreases gradually. The neighboring curve interval of the 2f signal amplitude decreases with the gas pressure increasing. The amplitude curves at different pressures do not intersect except for two curves at 600 and 700 Torr. This is due to the fact that in Doppler broadening (at low pressures), the spectral amplitude increases with the gas pressure increasing, while in a pressure broadening regime (at high pressures), the spectral amplitude is insensitive to the gas pressure. Hence an operating pressure of 600-700 Torr is optimum based on Fig. 4.

The SF$_6$ gas pressure in an electric power system is ~4,400 Torr, which is too high to implement the spectral measurement due to spectral broadening and the sensor requirement of a high pressure capacity. Therefore the gas pressure has to be reduced in order that the allowed pressure range before spectral measurement can be carried out. The Taiyuan area, China, has an atmospheric pressure of ~700 Torr as a result of its 784-m altitude. A straightforward way to deduce the pressure in field applications is to set an automatic reducing valve into the MGC, which can reduce the pressure to the outside atmospheric pressure. Therefore we selected the optimal modulation depth of 0.138 cm^{-1} at a pressure of 700 Torr according to the results in Fig. 4 in the following experiments, which corresponds to a modulation index of 2.3.
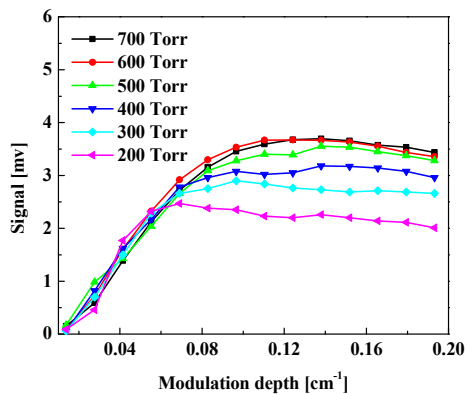

Fig. 4. Measured curve of 2f signal amplitude as a function of the modulation depths for a 20-ppm CO:SF$_6$ gas mixture as a function of operating gas pressure.

4.2 Spectral data processing method

For an online sensor system, a fast data output rate is desirable. Therefore, a 6 Hz saw tooth from function generator 1 was used to scan the 2.33 μm diode laser wavelength from 4284.9 cm^{-1} to 4285.2 cm^{-1}, while a 2 kHz sine wave from function generator 2 was employed to dither the laser wavelength with an optimal modulation depth of 10 mA, in order to simplify the hardware construction and reduce the workload of the acquisition system. The lock-in amplifier was set with a time constant of 3 ms and filter slope of 24 dB, corresponding to an equivalent noise bandwidth (ENBW) Δf = 26.04 Hz, according to its operating manual. It was verified that with such integration parameters the observed spectral lines were not only distorted by the lock-in detection, but also had a lower noise level. The sampling rate of the acquisition system triggered by sync signal from function generator 1 was set to 12 kHz.

The acquired CO spectrum was processed using a three-step algorithm. In the first step, a consecutive acquisition of 6,000 data points was carried out after the acquisition system was triggered, which included 3 complete CO spectra. In the second step, the 3 CO spectra were separated and averaged. In the third step, a standard CO 2f spectrum, which was calculated and stored in the computer memory in advance, was fitted to the averaging 2f spectra using a

Levenberg-Marquardt nonlinear least-squares fit procedure [26]. The fitting routine was written in Labview$^@$ code, which can output a scale factor between the standard and acquired CO spectra. The scale factor can retrieve the measured concentration value since the standard spectrum corresponds to the case of a 40 ppm CO concentration level.

The acquisition and signal processing time take 0.5 s and 0.4 s, respectively. A queue operation was adopted to implement the data acquisition and processing in parallel, resulting in a final data updating rate of the concentration value is 0.6 s/point. A fitting example of the 20-ppm CO 2f-WMS spectrum is shown in Fig. 5. The obtained scale factor is 0.499, which yields a measured concentration value of 19.97 ppm.
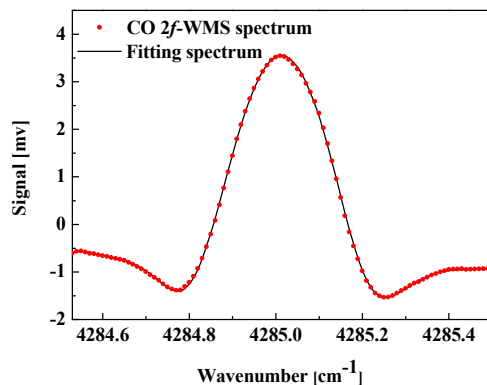

Fig. 5. A 20-ppm CO 2f-WMS spectrum (red dots); a fitting spectrum (black line) with a scale factor of 0.499 resulted in a measured concentration value of 19.97 ppm.

4.3 Flow response time

The flow response time is an important parameter especially for online sensor system, which is a function of flow, MGC volume and surface adsorption-desorption rate of the target gas molecule. The volume of the MGC is 0.9 L. The response time was investigated as a function of the flow rete. The MGC was initially filled with a constant concentration of CO:SF_6 gas mixture. Then pure SF_6 was used to flush the MGC at different flow rates. The measured concentration values were monitored during this process. The SF_6 molecules are heavy with a relative molecular mass of 146, considerably higher than the relative molecular mass of air, 29. As a result, the maximum flow rate was limited to 200 standard cubic centimeters per minute (SCCM), due to the fact that the mass flow controller designed for air or nitrogen. Figure 6 depicts the normalized concentration signal for different rates during the flushing process. It is obvious that the flushing time decreases with an increasing gas flow rate, due to the fact that a larger flow rate increases the gas exchange rate in the MGC. We define the parameter τ in the exponential decay fit of $e^{-t/\tau}$ to the normalized concentration signal curve as the flow response time. The response time of the sensor system was estimated to be 3 min, 4.2 min and 5.8 min for a fixed flow rate of 200 SCCM and 100 SCCM, 30 SCCM, respectively. If a larger flow rate is provided, a faster response time of the sensor system can be achieved.
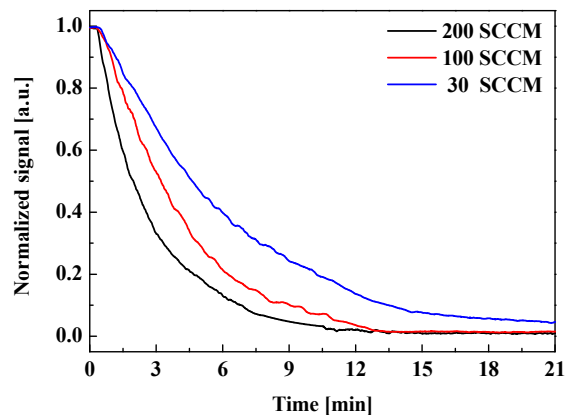
Fig. 6. Flow response time of the sensor system with pure SF$_6$ flushing at three different gas flow rates.

4.4 Sensor linearity, precision and stability

The linearity of the sensor system was first evaluated. The different concentration levels of CO, 40 ppm, 30 ppm, 20 ppm, 10 ppm and 6 ppm, were generated by diluting the certificated 500 ppm CO:SF$_6$ gas mixture using the gas dilution system and were directed into the sensor system in turn. 200 points were measured continuously for each concentration level. Then the SF$_6$ buffer gas and high purity N$_2$ were introduced into the sensor system for a small signal and zero baseline measurements. Figure 7(a) depicts the experimental results. The sensor exhibits an excellent performance in terms of signal stability for each constant concentration. The signal amplitude of the SF$_6$ buffer gas is 3.04 ppm which is in good agreement with the information from the SF$_6$ supplier. In order to check the real zero baseline level, the 'signal' from the high-purity N$_2$ with an amplitude of 1 ppm was also plotted in the Fig. 7(a). This can be explained by the fact that an etalon effect occurs in our sensor system. When there is no CO gas present, the Levenberg-Marquardt nonlinear least-squares fit procedure tries to fit an etalon pattern using the standard CO 2f spectrum and then returns a concentration value, which reflects the etalon level of the sensor system, i.e. the detection sensitivity is limited at 1 ppm. Data for each step are averaged and plotted against CO nominal concentrations in Fig. 7(b). A linear relationship with a R-square value of 0.9994 between the measured and nominal concentrations confirms the excellent linearity of the sensor response to CO concentrations.
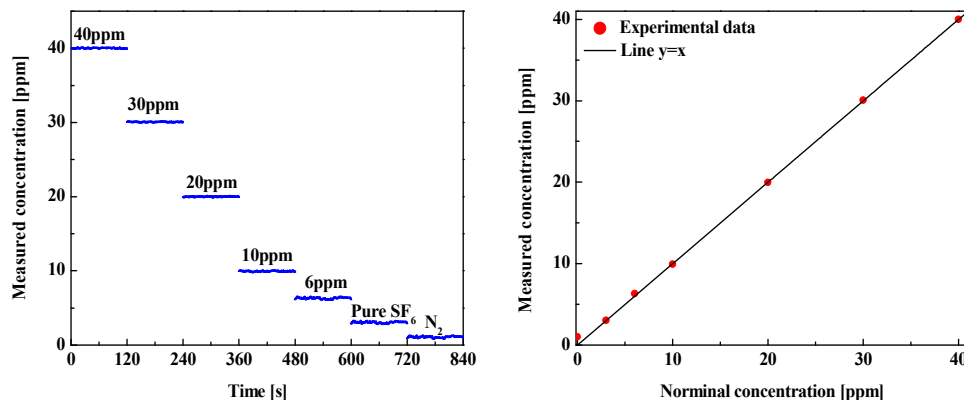

Fig. 7. (a) CO concentration response of the sensor system; (b) Linear dependence of the measured concentrations as a function of the five CO nominal concentrations.

To further examine the capabilities of the sensor system in terms of the measurement precision and the stability, time series measurements of 20 ppm $CO:SF_6$ gas mixture were carried out for 85 mins, which includes 8,500 concentration points. A histogram plot of measured concentrations depicting an approximate normal distribution around the mean value is plotted in Fig. 8, which can be used to assess the measurement precision. A Gaussian profile is fitted to the distribution histogram with a R-square value of 0.993, resulting in a half-width at half-maximum (HWHM) of 39 ppb and sigma value of 33 ppb with the concentration output rate of 0.6 s. This verifies that the sensor measurement precision is better than 40 ppb.
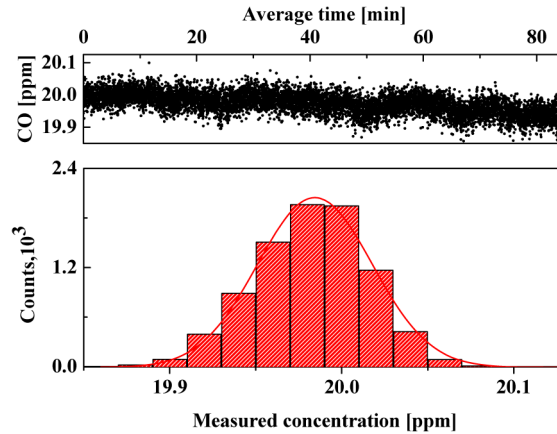

Fig. 8. Percent deviation of the measured concentration compared with the calculated value. Histogram plot of the deviation. The red line depicts a Gaussian profile.

The stability of the CO sensor system, characterized by the Allen-Werle variance, was investigated. Figure 9 shows the Allan-Werle variance obtained from the same time series measurements used in the histogram plot. When the averaging time is <48 s, the Allan-Werle variance follows a $1/\tau$ dependence during the duration of the measurement series, which indicates that thermal noise of the sensor system remains the dominant noise source in such a time scale. This yields an optimum averaging time of 48 s with a precision of ~6 ppb. In field applications, a faster flow rate of >200 SCCM can be set to match an optimum averaging time to achieve the optimum working status of the sensor system.
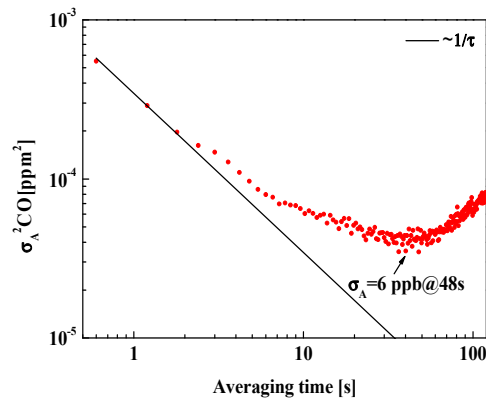

Fig. 9. Allan variance plot for the same time series measurements with the histogram plot.

5. Conclusions

In this work, we developed a ppm-level CO sensor system for a SF_6 decomposition analysis by use of a 2.33 μm DFB diode laser and a 14.5 m MGC. The challenge of quantifying CO concentration levels in SF_6 is to avoid the strong spectral interference from SF_6 absorption. The selection of the CO first overtone band for CO detection, where no SF_6 absorption behavior is observed and whose absorption coefficients are stronger than the CO second overtone band at 1.55 μm, is a compromise between the detection sensitivity, the spectral interference and cost efficiency. The identification of the optimal detection wavelength results in a minimum detection sensitivity of 1 ppm, which is limited by etalon effects from the MGC. Such a detection sensitivity is sufficient for online monitoring of electric power systems. A measurement precision of 40 ppb can be obtained with a concentration update rate of 0.6 s, while the precision can be improved to 6 ppb with an averaging time of 48 s. This is attributed to the use of a Levenberg-Marquardt nonlinear least-squares fit algorithm, in which the information from all data points based on the 2f-WMS spectrum is fully utilized. The flow rate effect was tested in the range of 30 SCCM to 200 SCCM due to the performance limitation of the gas dilution system. However, a higher flow rate matching the optimal averaging time of 48 s can make the sensor system to operate in its best condition in the field applications. Deployment of the sensor system in gas-insulated switchgear to further evaluate its performance for CO concentration monitoring in the field will be conducted in the near future.

References

1. R. Kurte, C. Beyer, H. M. Heise, and D. Klockow, "Application of infrared spectroscopy to monitoring gas insulated high-voltage equipment: electrode material-dependent SF_6 decomposition," Anal. Bioanal. Chem. **373**(7), 639–646 (2002).
2. E. Duffour, "Molecular dynamic simulations of the collision between copper ions, SF_6 molecules and a polyethylene surface: a study of decomposition products and an evaluation of the self-diffusion coefficients," Macromol. Theory Simul. **19**, 88–99 (2010).
3. J. Luo, Y. H. Fang, Y. D. Zhao, A. J. Wang, D. C. Li, Y. Y. Li, Y. Liu, F. X. Cui, J. Wu, and J. X. Liu, "Research on the detection of SF_6 decomposition products based on non-resonant photoacoustic spectroscopy," Anal. Methods **7**(3), 1200–1207 (2015).
4. H. Shinkai, H. Goshima, and M. Yashima, "A study on condition assessment method of gas-insulated switchgear. Part II. Influence of moisture in the SF_6, detection of a partial discharge on a spacer, repetition discharge and overheating by incomplete contact," Electr. Eng. Jpn. **176**(2), 22–30 (2011).
5. X. Yin, L. Dong, H. Wu, H. Zheng, W. Ma, L. Zhang, W. Yin, L. Xiao, S. Jia, and F. K. Tittel, "Highly sensitive SO_2 photoacoustic sensor for SF_6 decomposition detection using a compact mW-level diode-pumped solid-state laser emitting at 303 nm," Opt. Express **25**(26), 32561–32590 (2017).
6. X. L. Yan, G. Song, C. Y. Wang, Y. S. Ji, R. Yang, Y. F. Jian, and H. M. Liu, "Gas-insulated switchgear state monitoring based on SF_6 decomposition products detection," Electric power automation equipment. **34**(6), 83–88 (2014).
7. L. Dong, Y. Yu, C. Li, S. So, and F. K. Tittel, "Ppb-level formaldehyde detection using a CW room-temperature interband cascade laser and a miniature dense pattern multipass gas cell," Opt. Express **23**(15), 19821–19830 (2015).
8. K. Liu, L. Wang, T. Tan, G. S. Wang, W. J. Zhang, W. D. Chen, and X. M. Gao, ""Highly sensitive detection of methane by near-infrared laser absorption spectroscopy using a compact dense-pattern multipass cell," Sensor. Actuat. Biol. Chem. **220**, 1000–1005 (2015).

9. Y. Cao, N. P. Sanchez, W. Jiang, R. J. Griffin, F. Xie, L. C. Hughes, C. E. Zah, and F. K. Tittel, "Simultaneous atmospheric nitrous oxide, methane and water vapor detection with a single continuous wave quantum cascade laser," Opt. Express **23**(3), 2121–2132 (2015).

10. W. Ren, L. Q. Luo, and F. K. Tittel, "Sensitive detection of formaldehyde using an interband cascade laser near 3.6 um," Sensor. Actuat. Biol. Chem. **221**, 1062–1068 (2015).

11. C. G. Li, L. Dong, C. T. Zheng, and F. K. Tittel, "Compact TDLAS based optical sensor for ppb-level ethane detection by use of a 3.34 um room-temperature CW interband cascade laser," Sensor. Actuat. Biol. Chem. **232**, 188–194 (2016).

12. W. Ye, C. Li, C. Zheng, N. P. Sanchez, A. K. Gluszek, A. J. Hudzikowski, L. Dong, R. J. Griffin, and F. K. Tittel, "Mid-infrared dual-gas sensor for simultaneous detection of methane and ethane using a single continuous-wave interband cascade laser," Opt. Express **24**(15), 16973–16985 (2016).

13. F. Wang, N. Li, Q. X. Huang, J. H. Yan, and K. F. Cen, "Measurements on CO concentration and gas temperature at 1.58 um with tunable diode laser absorption spectroscopy," AIP Conf. Proc. **914**, 499–508 (2007).

14. X. Chao, J. B. Jeffries, and R. K. Hanson, "Absorption sensor for CO in combustion gases using 2.3 μm tunable diode lasers," Meas. Sci. Technol. **20**(11), 5201–5210 (2009).

15. J. M. Dang, H. Y. Yu, Y. J. Sun, and Y. D. Wang, "A CO trace gas detection system based on continuous wave DFB-QCL," Infrared Phys. Technol. **82**, 183–191 (2017).

16. R. Ghorbani and F. M. Schmidt, "ICL-based TDLAS sensor for real-time breath gas analysis of carbon monoxide isotopes," Opt. Express **25**(11), 12743–12752 (2017).

17. Y. Ma, R. Lewicki, M. Razeghi, and F. K. Tittel, "QEPAS based ppb-level detection of CO and N_2O using a high power CW DFB-QCL," Opt. Express **21**(1), 1008–1019 (2013).

18. L. Dong, R. Lewicki, K. Liu, P. R. Buerki, M. J. Weida, and F. K. Tittel, "Ultra-sensitive carbon monoxide detection by using EC-QCL based quartz-enhanced photoacoustic spectroscopy," Appl. Phys. B **107**(2), 275–283 (2012).

19. Y. F. Ma, G. Yu, J. B. Zhang, X. Yu, and R. Sun, "Sensitive detection of carbon monoxide based on a QEPAS sensor with a 2.3 μm fiber-coupled antimonide diode laser," J. Opt. **17**(5), 055401 (2015).

20. Z. L. Li, Z. Wang, Y. Qi, W. Jin, and W. Ren, "Improved evanescent-wave quartz-enhanced photoacoustic CO sensor using an optical fiber taper," Sensor. Actuat. Biol. Chem. **248**, 1023–1028 (2017).

21. X. Yin, L. Dong, H. Zheng, X. Liu, H. Wu, Y. Yang, W. Ma, L. Zhang, W. Yin, L. Xiao, and S. Jia, "Impact of humidity on quartz-enhanced photoacoustic spectroscopy based co detection using a near-ir telecommunication diode laser," Sensors (Basel) **16**(2), 162 (2016).

22. D. S. Bomse, A. C. Stanton, and J. A. Silver, "Frequency modulation and wavelength modulation spectroscopies: comparison of experimental methods using a lead-salt diode laser," Appl. Opt. **31**(6), 718–731 (1992).

23. J. Li, U. Parchatka, R. Königstedt, and H. Fischer, "Real-time measurements of atmospheric CO using a continuous-wave room temperature quantum cascade laser based spectrometer," Opt. Express **20**(7), 7590–7601 (2012).

24. F. K. Tittel, J. J. Allred, Y. Cao, N. P. Sanchez, W. Ren, W. Jiang, D. F. Jiang, and R. J. Griffin, "Quantum cascade laser-based sensor system for nitric oxide detection, SPIE, OPTO," Int. Soc. Opt. Photonics. **9370**, 93700–93707 (2015).

25. Z. Wang, Z. Li, and W. Ren, "Quartz-enhanced photoacoustic detection of ethylene using a 10.5 μm quantum cascade laser," Opt. Express **24**(4), 4143–4154 (2016).

26. J. J. Moré, "The Levenberg-Marquardt algorithm: implementation and theory," in Numerical analysis, G. A. Watson, ed. (Springer, 1978).